*Progress In Electromagnetics Research M, Vol. 79, 199–207, 2019*

# Planar Endfire Circularly Polarized Quasi-Yagi Antenna with Enhanced Bandwidth and Reduced Size for Wideband Wireless Applications

**Tian Li***

**Abstract**—A planar endfire circularly polarized quasi-Yagi antenna with the feasibility of obtaining a wider bandwidth and relatively smaller size is proposed and demonstrated. With a planar double-sided printed complementary structure, the proposed endfire circularly polarized (CP) antenna, consisting of a vertically polarized planar quasi-Yagi array and a horizontally polarized planar quasi-Yagi array with a common driver, is designed, analyzed, and fabricated. Good agreement between simulated and measured results is observed. Simulation and measurement results reveal that the proposed antenna can provide an impedance bandwidth of 16.3% (5.02–5.91 GHz) and a 3 dB axial ratio (AR) bandwidth of 17.4% (5–5.95 GHz). Meanwhile, the proposed antenna has endfire gains from 5.4 dBic to 7.4 dBic with an average endfire gain of 6.3 dBic, and front-to-back (F/B) ratios ranging from 10.2 dB to 16 dB with an average F/B ratio of 11.9 dB. Additionally, the measured effective CP bandwidth of 16.3% (5.02–5.91 GHz) not only meets the need for certain Wi-Fi (5.2/5.8 GHz) or WiMAX (5.5 GHz) band communication application, but also provides the potential to implement multiservice transmission.

## 1. INTRODUCTION

Planar circularly polarized (CP) antennas have attracted great attention due to their merits of simple structure, low profile, light weight, low fabrication cost, low loss, capabilities of reducing polarization mismatch, suppressing multipath interferences, and suitability for integration with microwave circuits. Compared with the conventional planar microstrip CP antennas with the main beams at broadside, planar endfire CP quasi-Yagi antennas can provide endfire CP beams in parallel with the antenna plane and broader bandwidth due to their inherent quasi-Yagi structures [1–10]. On the one hand, though the feature of broad 3 dB axial ratio (AR) bandwidth is becoming increasingly necessary due to the high data rate required by modern services, many newly published planar endfire CP antennas in [6–8] only support narrow-band applications. In [6], a planar endfire circularly polarized antenna with an effective CP bandwidth of 2.4% is presented based on a pair of orthogonally combined magnetic dipoles, and it is $1.11\lambda_0 \times 1.05\lambda_0$ in size. In [7], a planar dipole-aperture combined antenna with endfire circularly polarized radiation is introduced, and it obtains an effective CP bandwidth of 1.9% and a very compact size of $0.73\lambda_0 \times 0.59\lambda_0$. Moreover, in [8], a planar loop-aperture combined antenna with endfire CP radiation is presented, which obtains an effective CP bandwidth of 8.0% and a compact size of $0.74\lambda_0 \times 0.65\lambda_0$. All the three planar endfire CP antennas presented in [6–8] have a lower profile of $0.04\lambda_0$. However, their gains of 2.6 dBc, 2.3 dBc and 1.5 dBc as well as their effective CP bandwidths are limited. On the other hand, the planar helical antennas in [9] and [10] have relatively higher profiles due to their helical structures. In [9], a planar helical antenna with straight-edge connections implemented by plated via-holes is presented. The antenna has a wide effective CP bandwidth of 34% with a large

*Received 1 February 2019, Accepted 19 March 2019, Scheduled 29 March 2019*
* Corresponding author: Tian Li (tianli@stu.xidian.edu.cn).
The author is with the Southwest China Institute of Electronic Technology, Chengdu 610036, P. R. China.

size of $1.22\lambda_0 \times 1.25\lambda_0$, and its profile is $0.11\lambda_0$. In [10], a millimeter-wave CP SIW endfire bow-tie antenna utilizing semi-planar helix unit cell is proposed. It has an effective CP bandwidth of 17.4% and a profile of $0.1\lambda_0$.

In this paper, a relatively compact planar endfire circularly polarized quasi-Yagi antenna with a measured effective CP bandwidth of 16.3% and a size of $1.11\lambda_0 \times 1.05\lambda_0 \times 0.046\lambda_0$ is presented. The proposed antenna is based on a complementary antenna combining a vertically polarized printed magnetic dipole and a horizontally polarized printed electric dipole, with a balanced phase shift line located between them to provide 90° phase difference, thus obtaining endfire CP characteristic. To improve the bandwidth and gain, a vertically polarized and a horizontally polarized quasi-Yagi arrays are introduced, and this complementary antenna mainly accounting for the CP radiation acts as their common driver. The phase shift line of the driver utilizes two-stage stepped structure so as to broaden the antenna AR bandwidth. Meanwhile, two rectangular slots are symmetrically loaded on the metal ground of the vertically polarized driver, which facilitates the shift of impedance band towards the lower band, thus contributing to a relatively compact size. Furthermore, two meandered arc-shaped slots are loaded on the horizontally polarized driver, which effectively improves the impedance performance, especially for the lower frequencies. Finally, a pair of shorting vias is loaded on the vertically polarized reflector to further improve the impedance performance. For demonstration, the proposed antenna is fabricated and measured. The measured results have a reasonable agreement with the simulated ones.

## 2. ANTENNA CONFIGURATION

Figure 1 shows the geometry of the proposed planar endfire circularly polarized quasi-Yagi antenna. The substrate has a relative dielectric constant of 2.2, loss tangent of 0.0009, surface area size of 60.9 mm × 57.7 mm and height of 2.54 mm (100 mil). The common driver can be divided into three parts, namely magnetic dipole, electric dipole and phase shift line. The magnetic dipole element is realized by a microstrip patch with one long edge opened and the other three edges shorted. For fabrication convenience, several rows of closely-spaced shorting pins penetrating through the proposed antenna are employed to replace the ideal shorting walls. The shorting pins have a radius of 0.33 mm and a distances of 1.78 mm. The magnetic dipole is 60.9 mm × 10.3 mm in size. And two rectangular slots with sizes of 5.5 mm × 0.4 mm are symmetrically loaded on the metal ground of the magnetic dipole. The electric dipole's two arms are printed on the front and back sides of the substrate complementarily. Each arm has a size of 12.9 mm × 4.4 mm, and a meandered slot composed of three identical arc-shaped slots is loaded on it. The radius of two arc-shaped slots is 1.2 mm. Meanwhile, the sizes of the two-stage stepped balanced phase shift line are 9.3 mm × 1.25 mm and 5 mm × 0.85 mm, respectively. The feeding

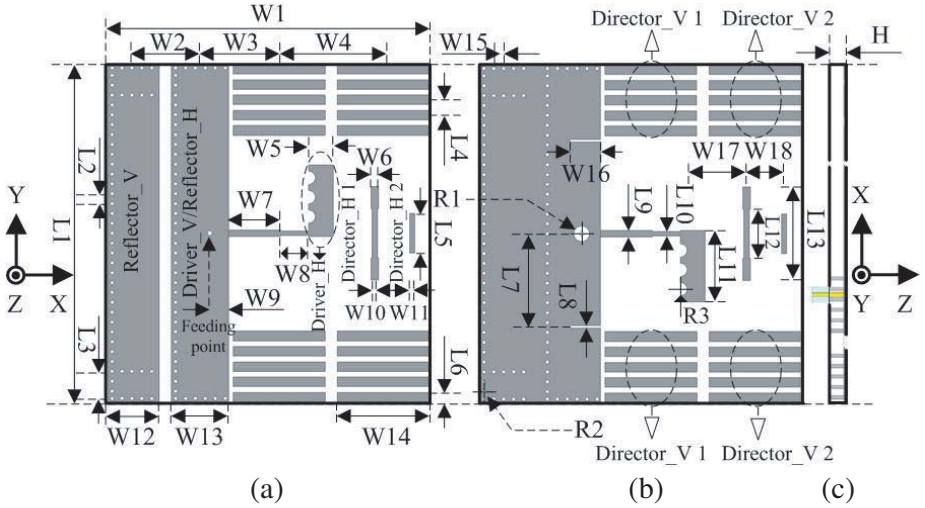


**Figure 1.** Configuration of the proposed antenna. (a) Front view; (b) back view; (c) side view.

point locates in the center of the common driver in lateral direction and has a distance of 3.4 mm from the magnetic dipole's opened edge. Moreover, the vertically polarized reflector is 60.9 mm × 9.3 mm in size. Both vertically and horizontally polarized directors consist of two stages printed both sides of the substrate symmetrically. The two identical stages of the vertically polarized director have a distance of 18.7 mm. And each stage consists of five parallel parasitic patch element with the size of 16.5 mm × 1.74 mm and the spacing of 2.76 mm. Furthermore, the horizontally polarized director employs tapered structure. The first stage has a length of 10.3 mm and stepped widths of 1.35 mm and 0.95 mm. Its second stage is 7.1 mm × 0.9 mm in size. Finally, a pair of shorting vias is loaded on the vertically polarized reflector, which has a distance of 4.9 mm from its short shorted edges. The detailed geometry and dimensions of the proposed antenna are given in Figure 1 and Table 1.

**Table 1.** Dimensions of the proposed antenna (unit: mm).

| Parameter | Value | Parameter | Value | Parameter | Value |
|---|---|---|---|---|---|
| $L1$ | 60.9 | $L13$ | 16.9 | $W12$ | 9.3 |
| $L2$ | 1.78 | $W1$ | 57.7 | $W13$ | 10.3 |
| $L3$ | 4.9 | $W2$ | 11.95 | $W14$ | 16.5 |
| $L4$ | 2.76 | $W3$ | 14.15 | $W15$ | 1.78 |
| $L5$ | 7.1 | $W4$ | 18.7 | $W16$ | 5.5 |
| $L6$ | 1.74 | $W5$ | 4.4 | $W17$ | 9.7 |
| $L7$ | 16.8 | $W6$ | 1.35 | $W18$ | 6.7 |
| $L8$ | 0.4 | $W7$ | 9.3 | $R1$ | 1.4 |
| $L9$ | 1.25 | $W8$ | 5 | $R2$ | 0.33 |
| $L10$ | 0.85 | $W9$ | 3.4 | $R3$ | 1.2 |
| $L11$ | 12.9 | $W10$ | 0.95 | $H$ | 2.54 |
| $L12$ | 9 | $W11$ | 0.9 | | |

## 3. ANTENNA DESIGN

The common driver element is a combined radiator, consisting of a magnetic dipole acting as the vertically polarized driver, an electric dipole acting as the horizontally polarized driver and their connecting line acting as the phase shift line. The magnetic dipole is based on a rectangular microstrip patch with one long edge opened and the other three edges shorted. And the long shorted edge enables the rectangular microstrip antenna to be a magnetic element, which provides vertically polarized radiation at endfire. While the other two shorted edges are extra designs to prevent propagation or leakage at these ends. Meanwhile, the patch has a longitudinal size along $+X$-axis direction of normally $\lambda_{g0}/4$ and a lateral size along $+Y$-axis direction of about one wavelength. Moreover, since the electric dipole has a complementary radiation pattern and orthogonal polarization with the magnetic dipole, if 90° phase difference is provided by the phase shift line, end-fire CP characteristic can be achieved while maintaining a planar structure. Furthermore, when supposing the continuity of the probe current path, the probe current flows from the upper patch of the magnetic dipole to the top layer of the phase shift line and the top arm of the printed dipole, and then the displacement current turns back to the bottom arm printed dipole and the bottom layer of the phase shift line, and finally return to the bottom layer of the magnetic dipole. Since the virtual probe current's path obeys a left-handed helix direction with thumb point at $+z$-direction, the proposed antenna operates in LHCP.

The common driver is energized directly with a backed soldered SMA connector, while the reflectors and directors act as parasitic radiators whose currents are induced by mutual coupling. The magnetic dipole behind the common driven element serves as the vertically polarized reflector, while the upper

patch and bottom layer of the magnetic dipole in the common driver serves as the horizontally polarized reflector. To broaden the antenna bandwidth, the phase shift line of the driver employs two-stage stepped structure, which effectively broadens the AR bandwidth [11]. Meanwhile, the meandered arc-shaped slots etched on the electric dipole in the common driver provide a slightly longer pathway for the current within a same total physical size, which effectively improves the impedance performance, especially for the lower frequencies [12]. Furthermore, two rectangular slots are symmetrically loaded on the metal ground of the vertically polarized driver acting as a perturbation structure to facilitate the shift of impedance band towards lower band. Finally, a pair of shorting vias is loaded on the vertically polarized reflector to break the surface current distribution balance, thereby further enhancing the impedance bandwidth.

## 4. SIMULATED AND MEASURED RESULTS

In order to facilitate the manufacture, the proposed antenna with the parameters shown in Figure 1 is fabricated and measured. The proposed antenna's measured and simulated VSWRs are depicted in Figure 2. Good agreement between the simulated results after optimization using ANSYS HFSS and measured ones is obtained. The simulated and measured impedance bandwidths (VSWR $\leq$ 2) of the proposed antenna are 15.5% (5.05–5.9 GHz) and 16.3% (5.02–5.91 GHz), respectively.

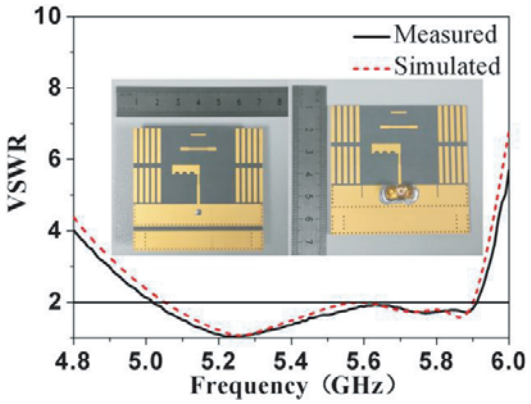


**Figure 2.** Simulated and measured VSWRs and the photographs of the fabricated antenna.

Figure 3 shows the simulated and measured normalized radiation patterns in the $XY$-plane and $XZ$-plane at 5.2, 5.5 and 5.8 GHz, with front-to-back (F/B) ratios of 11.3 dB, 11.8 dB and 12.1 dB respectively. In Figure 4, the measured endfire gains are from 5.4 dBic to 7.4 dBic with an average endfire gain of 6.3 dBic. From Figure 3 and Figure 4, it can be seen that relatively stable pattern characteristics are obtained. Meanwhile, the simulated and measured 3-dB AR bandwidths (AR $\leq$ 3) are 17.2% (5–5.94 GHz) and 17.4% (5–5.95 GHz), respectively. It should be noted that the discrepancy between the simulated and measured results may be caused by the imperfect testing environment, which is mainly due to the interferences from indoor reflection. Furthermore, the errors in the process of fabrication, namely the errors resulting from limited processing accuracy and the errors of un-uniformity of the substrate with respect to relative dielectric constant and loss tangent, and the presence of the SMA connector interfering with the radiated field may be taken into account as well. In addition, the measured effective CP bandwidth of 16.3% (5.02–5.91 GHz) not only includes certain Wi-Fi (5.2/5.8 GHz) or WiMAX (5.5 GHz) band communication application, but also offers the potential to implement multiservice transmission.

A comparison of the proposed antenna with published referenced work is made in terms of effective CP bandwidth, relative dielectric constant of the substrate, antenna height, bandwidth and peak gain with results presented in Table 2. The selected criteria for inclusion in this comparison are newly published planar endfire circularly polarized antennas. Compared with the antennas presented in [6, 7] and [8], the proposed antenna obtains a much wider effective CP bandwidth and higher gain, without

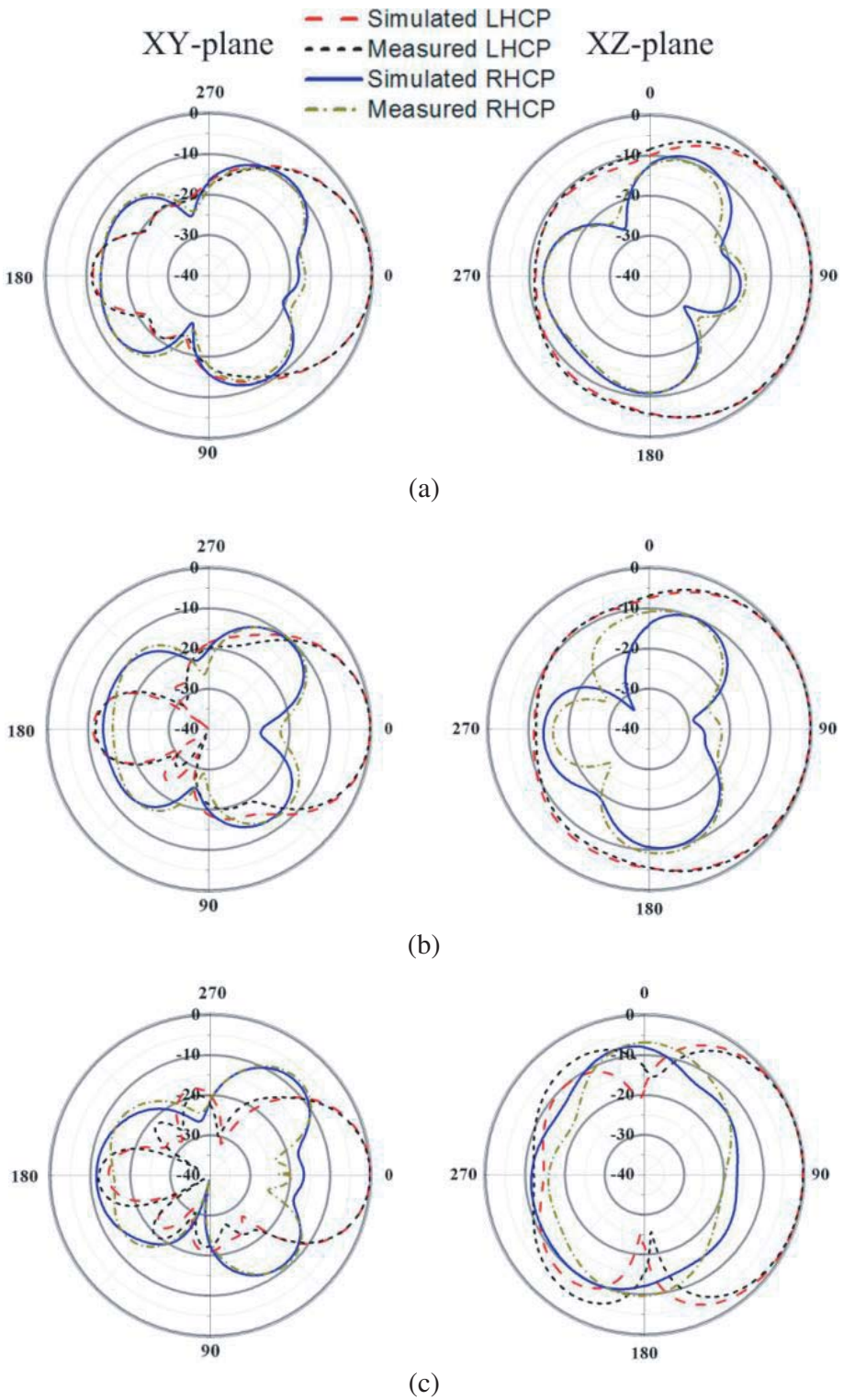


**Figure 3.** Simulated and measured radiation patterns in the $XY$-plane and $XZ$-plane. (a) 5.2 GHz; (b) 5.5 GHz; (c) 5.8 GHz.

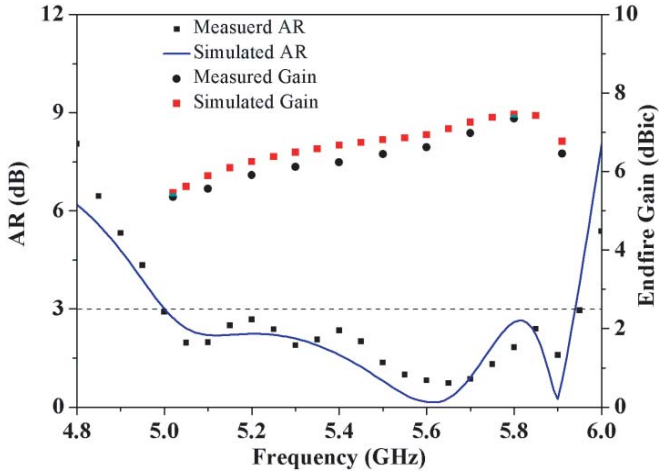


**Figure 4.** Simulated and measured ARs and endfire gains of the proposed antenna.

**Table 2.** Comparison of the proposed and referenced antennas. (BW: Effective CP bandwidth).

| Reference Designs | BW (GHz) | Substrate $\varepsilon_r$ | Antenna height (mm) | Peak gain (dBic) |
|---|---|---|---|---|
| **Proposed Antenna** | 5.02–5.91 (16.3%) | 2.2 | 2.54 ($0.046\lambda_0$) | 7.4 dBic at 5.8 GHz |
| **Lu et al. [6]** | 5.74–5.88 (2.4%) | 2.65 | 2.0 ($0.04\lambda_0$) | 2.6 dBic at 5.8 GHz |
| **Zhang et al. [7]** | 5.75–5.86 (1.9%) | 2.65 | 2.0 ($0.04\lambda_0$) | 2.3 dBic at 5.8 GHz |
| **You et al. [8]** | 8.0% around 2.45 GHz | 1.1 | 5.0 ($0.04\lambda_0$) | about 1.5 dBic |
| **Chen et al. [9]** | 8.2–11.6 (34%) | 2.2 | 3.175 ($0.11\lambda_0$) | about 10 dBic |
| **Rafiei et al. [10]** | 54–64.3 (17.4%) | 2.2 | 0.5 ($0.1\lambda_0$) | 12.5 dBic at 58 GHz |

sacrificing the antenna profile performance significantly. Meanwhile, though the antennas presented in [9] and [10] have an inherent advantage on the proposed antenna in effective CP bandwidth, their antenna profiles are much higher than that of the proposed antenna due to their helix structures. Consequently, from Table 1, it could be seen that the proposed antenna provides either a wider effective CP bandwidth or a lower profile. Actually, it obtains a better performance with a favorable compromise between operating bandwidth and antenna profile.

## 5. PARAMETRIC STUDY

All critical physical parameters, such as $L7, R3, W9, W8, L3, W14, W3$ and $W17$, should be adjusted carefully to achieve a good performance. In this section, the effects of these parameters on impedance and AR bandwidths are examined in detail to facilitate the design of a similar antenna with different specifications. During this process, all the other parameters not mentioned stay constant as shown in Table 1.

### 5.1. Effect of the Vertically and Horizontally Polarized Drivers ($L7$ and $R3$)

The effects of two rectangular slots and the meandered arc-shaped slots etched on the vertically and horizontally polarized drivers ($L7$ and $R3$) on the impedance and AR bandwidths are shown in Figure 5 and Figure 6, respectively. When two rectangular slots are introduced with discreetly optimized distances of 16.8 mm from the feeding point, the whole impedance and AR bandwidths shift toward lower band, which facilitates the proposed antenna's miniaturization. Meanwhile, with two meandered arc-shaped slots, as $R3$ increases, the whole impedance bandwidth will be broadened, especially for the

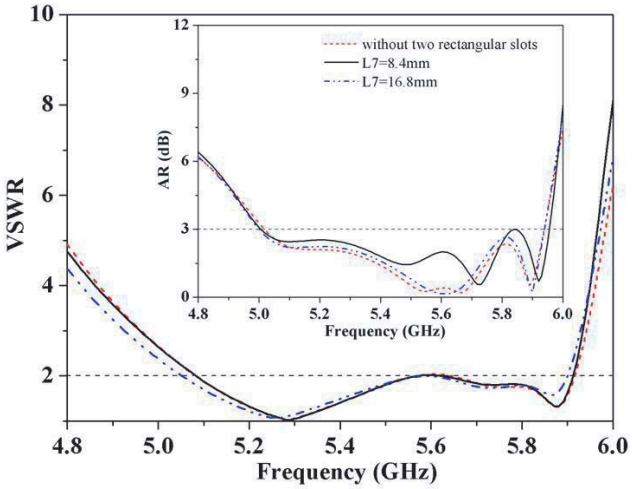


**Figure 5.** VSWRs and ARs with varied $L7$.

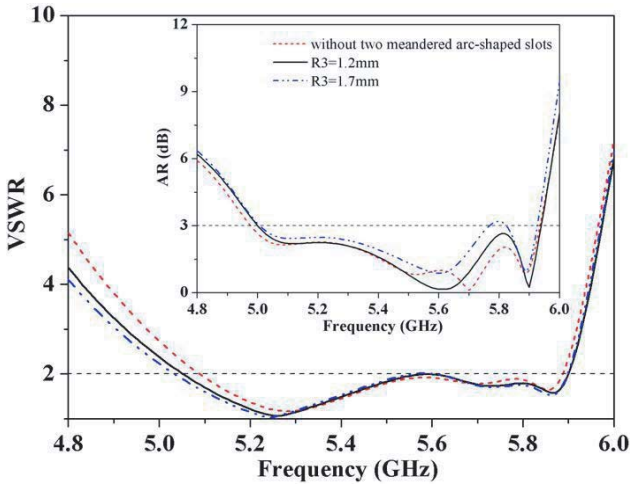


**Figure 6.** VSWRs and ARs with varied $R3$.

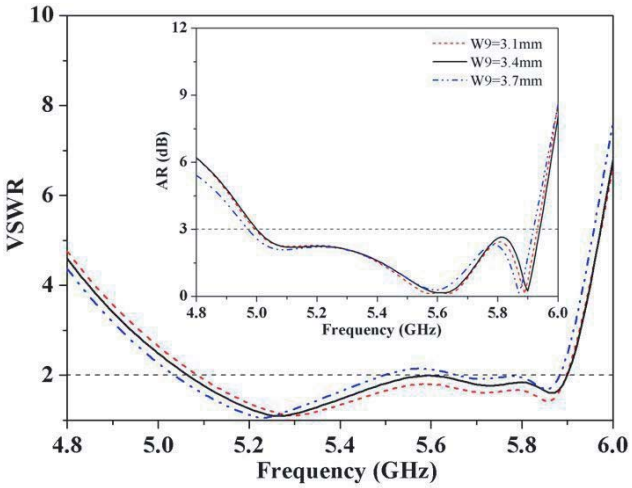


**Figure 7.** VSWRs and ARs with varied $W9$.

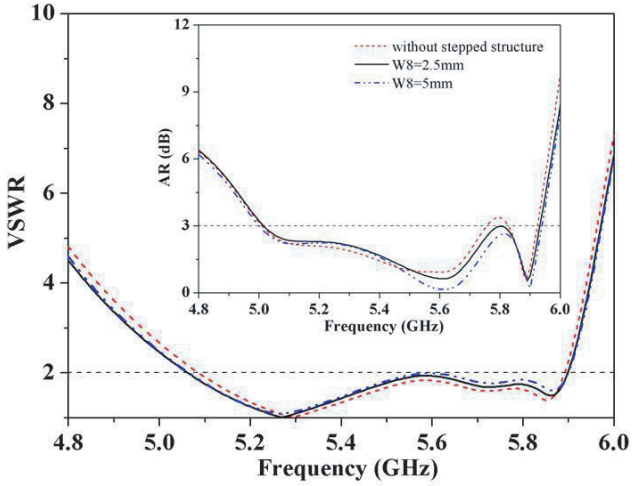


**Figure 8.** VSWRs and ARs with varied $W8$.

lower band, whereas the AR bandwidth will degrade simultaneously. To obtain a wider effective CP bandwidth, $R3$ is set as 1.2 mm ultimately.

### 5.2. Effect of the Feeding Point and the Phase Shift Line ($W9$ and $W8$)

Figure 7 and Figure 8 reveal the influence of the feeding point and phase shift line ($W9$ and $W8$) on the impedance and AR bandwidths. As $W9$ increases, the impedance bandwidth shifts toward lower band. While the AR bandwidth will shift toward lower band, whether the value increases or decreases. Moreover, with stepped phase shift line, as $W8$ increases, the whole AR bandwidth will be broadened effectively, while the impedance bandwidth almost stays the same. To obtain good impedance matching and AR performance, $W9$ and $W8$ are set as 3.4 mm and 5 mm, respectively.

### 5.3. Effect of the Vertically Polarized Reflector and Director ($L3$ and $W14$)

The effects of the vertically polarized reflector and director ($L3$ and $W14$) on the impedance and AR bandwidths are shown in Figure 9 and Figure 10, respectively. As shown in Figure 9, the presence of

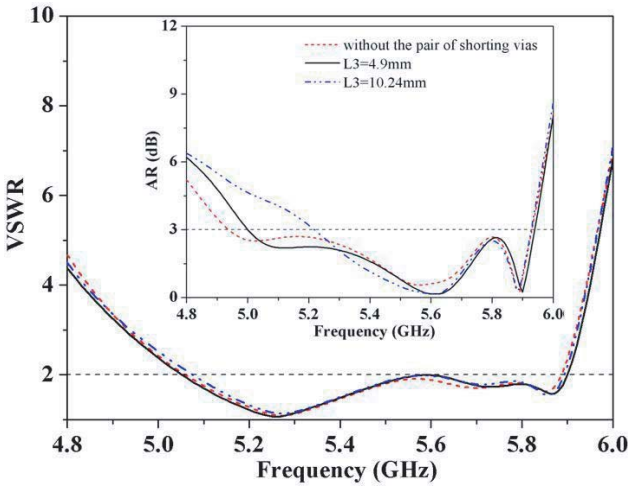


**Figure 9.** VSWRs and ARs with varied $L3$.

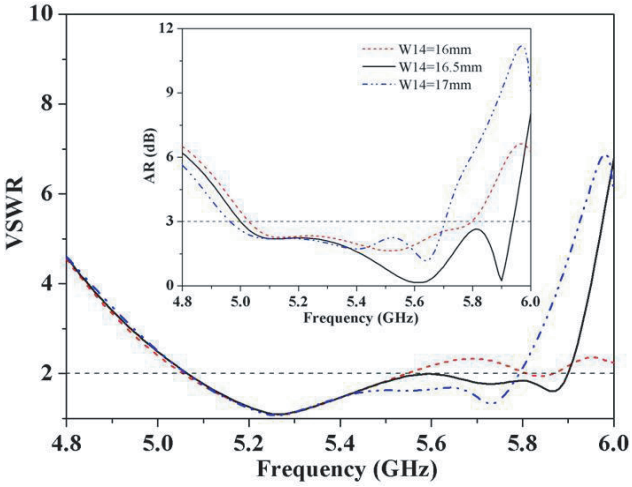


**Figure 10.** VSWRs and ARs with varied $W14$.

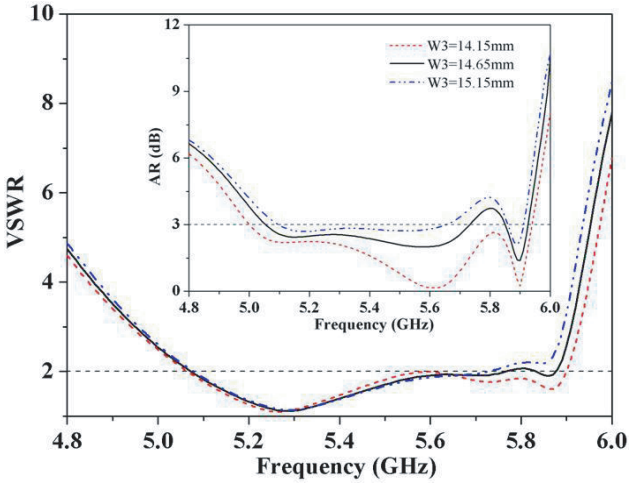


**Figure 11.** VSWRs and ARs with varied $W3$.

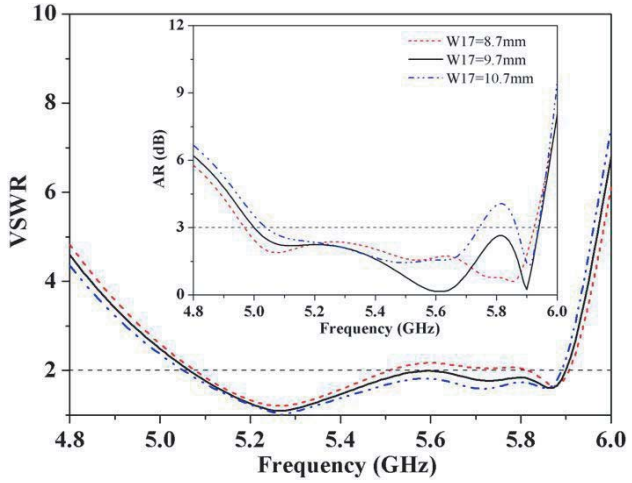


**Figure 12.** VSWRs and ARs with varied $W17$.

the pair of shorting vias, which is loaded on the vertically polarized reflector, can effectively increase the antenna impedance bandwidth. Meanwhile, as shown in Figure 10, both the impedance and AR bandwidths at higher band are sensitive to the length of the vertically polarized director element. To obtain good impedance matching and AR performance, $L3$ and $W14$ are carefully tuned as 4.9 mm and 16.5 mm, respectively.

### 5.4. Effect of the Distance of the Vertically and Horizontally Polarized Drivers and Directors ($W3$ and $W17$)

Figure 11 and Figure 12 reveal the influence of the distance of the vertically and horizontally polarized drivers and directors ($W3$ and $W17$) on the impedance and AR bandwidths, respectively. As $W3$ increases, both the impedance and AR bandwidths will be deteriorated. Furthermore, as $W17$ increases, the impedance bandwidth shifts toward lower band. Simultaneously, the AR bandwidth will shift toward upper band, while the AR performance at higher frequencies will be deteriorated, whether the value increases or decreases. To obtain good impedance matching and AR performance, $W3$ and $W17$ are set as 14.15 mm and 9.7 mm, respectively.

## 6. CONCLUSION

A planar endfire CP quasi-Yagi antenna with enhanced impedance and reduced size has been presented. Simulation and measurement results indicate that with two compactly combined vertically and horizontally polarized planar quasi-Yagi arrays, the proposed antenna can produce an impedance bandwidth of 16.3% (5.02–5.91 GHz) and a 3 dB axial ratio (AR) bandwidth of 17.4% (5–5.95 GHz). The effects of all critical parameters on impedance and AR bandwidths are studied in detail to facilitate the design of a similar antenna. Meanwhile, within the effective CP bandwidth of 16.3% (5.02–5.91 GHz), good F/B ratios, which are better than 10.2 dB, are obtained. Relatively moderate endfire gains, ranging from 5.4 dBic to 7.4 dBic with an average gain of 6.3 dBic, are yielded simultaneously. With these inherent characteristics, the proposed planar endfire CP quasi-Yagi antenna can be a good candidate for wideband wireless applications.

## REFERENCES

1. Liu, J.-H. and Q. Xue, "Microstrip magnetic dipole Yagi array antenna with endfire radiation and vertical polarization," *IEEE Trans. Antennas Propag.*, Vol. 61, No. 3, 1140–1147, Mar. 2013.
2. Yang, Z.-Q., L.-M. Zhang, and T. Yang, "A microstrip magnetic dipole Yagi-Uda antenna employing vertical I-shaped resonators as parasitic elements," *IEEE Trans. Antennas Propag.*, Vol. 66, No. 8, 3910–3917, Aug. 2018.
3. Zhang, W.-H., P. Cheong, W.-J. Lu, and K.-W. Tam, "Planar endfire circularly polarized antenna for low profile handheld RFID reader," *IEEE Trans. Antennas Propag.*, Vol. 2, No. 1, 15–22, Mar. 2018.
4. Yang, H.-Q., M. You, W.-J. Lu, L. Zhu, and H.-B. Zhu, "Envisioning an endfire circularly polarized antenna: Presenting a planar antenna with a wide beamwidth and enhanced front-to-back ratio," *IEEE Mag. on Antennas Propag.*, Vol. 60, No. 4, 70–79, Aug. 2018.
5. Yaghjian, A.-D. and R.-B. Steven, "Impedance, bandwidth, and Q of antennas," *IEEE Antennas and Propagation Society International Symposium*, Vol. 1, 501–504, 2003.
6. Lu, W.-J., J.-W. Shi, K.-F. Tong, and H.-B. Zhu, "Planar endfire circularly polarized antenna using combined magnetic dipoles," *IEEE Antennas Wireless Propag. Lett.*, Vol. 14, 1263–1266, 2015.
7. Zhang, W.-H., W.-J. Lu, and K.-W. Tam, "A planar end-fire circularly polarized complementary antenna with beam in parallel with its plane," *IEEE Trans. Antennas Propag.*, Vol. 64, No. 3, 1146–1152, Mar. 2016.
8. You, M., W.-J. Lu, B. Xue, L. Zhu, and H.-B. Zhu, "A novel planar endfire circularly polarized antennawith wide axial-ratio beamwidth and wide impedance bandwidth," *IEEE Trans. Antennas Propag.*, Vol. 64, No. 10, 4554–4559, Oct. 2016.
9. Chen, Z.-Z. and Z.-X. Shen, "Planar helical antenna of circular polarization," *IEEE Trans. Antennas Propag.*, Vol. 63, No. 10, 4315–4323, Oct. 2015.
10. Rafiei, V., S. Karamzadeh, and H. Saygin, "Millimetre-wave high-gain circularly polarised SIW end-fire bow-tie antenna by utilising semi-planar helix unit cell," *Electron. Lett.*, Vol. 54, No. 7, 411–412, Apr. 2018.
11. Wu, J. N., Z.-Q. Zhao, Z.-P. Nie, and Q.-H. Liu, "Design of a wideband planar printed quasi-yagi antenna using stepped connection structure," *IEEE Trans. Antennas Propag.*, Vol. 62, No. 6, 3431–3435, Jun. 2014.
12. Podilchak, S.-K., J.-C. Johnstone, M. Clénet, and Y. M. M. Antar, "A compact wideband dielectric resonator antenna with a meandered slot ring and cavity backing," *IEEE Antennas Wireless Propag. Lett.*, Vol. 15, 909–913, 2016.